THE AMERICAN SOCIETY OF MECHANICAL ENGINEERS
345 E. 47 St., New York, N.Y. 10017

84-GT-15

EXPERIMENTAL STUDY OF THE FLOW FIELD BEHIND AN ANNULAR TURBINE NOZZLE GUIDE VANE WITH AND WITHOUT DOWNSTREAM ROTOR

E. Boletis and C.H. Sieverding
von Karman Institute for Fluid Dynamics
B - 1640 Rhode Saint Genèse, Belgium

ABSTRACT

Measurements of the three dimensional flow field in annular turbine nozzle guide vanes present an important step in the simulation of the real flow conditions in turbomachinery bladings. This paper seeks to determine whether the installation of a rotor closely behind a high hub-to-tip ratio cascade (D_H/D_T=0.8) is indispensable for establishing correct flow conditions at the cascade exit or whether the use of an axial diffuser of a certain length is sufficient. Also, an attempt is made to separate the possible effects of the rotor blades from that of the rotating rotor disc.

The tests are carried out on a low speed, low aspect ratio, high turning nozzle guide vane. The flow is explored by means of a double head four-hole pressure probe and the results are presented in the form of contour plots and spanwise pitch-averaged distributions of losses, flow angles and static pressure.

NOMENCLATURE

C	chord
CP_0	local total pressure coefficient, $(P_{01,MS}-P_{0,\ell})/(P_{01,MS}-\bar{P}_{s,2})$
$\overline{CP_0}$	total pressure loss, $(P_{01,MS}-\bar{P}_{0,2})/(P_{01,MS}-\bar{P}_{s,2})$
CP_s	local static pressure coefficient $(P_{01,MS}-P_{s,\ell})/(P_{01,MS}-\bar{P}_{s,2})$
D	diameter
g	pitch
H	blade height
$H_{1,2}$	boundary layer form factor
N	rotational speed, number of blades
O	throat
P	pressure
Re	Reynolds number, $Re = C_S \star V/\nu$
T	temperature
Tu	turbulence level, $Tu = \sqrt{\overline{v_{ax}^2}}/V_{MS}$
U	peripheral velocity of rotating hub end wall
V	velocity
v'	velocity fluctuation
X,Y	coordinates (Fig. 3)
α	flow angle in blade-to-blade plane (referred to axial direction)
α'	blade angle (angle between tangent to camberline and axial direction)
β	flow angle relative to the rotor (referred to the axial direction)
γ	radial flow angle, $\gamma = \text{arctg}\,(V_r/V_{ax})$
δ	boundary layer thickness
δ	boundary layer displacement thickness
η	mass flow coefficient, $\eta = \dfrac{\left(\int_{D_H}^{D_T} \rho \bar{V}_{ax} dr\right)_2}{\left(\int_{D_H}^{D_T} \rho \bar{V}_{ax} dr\right)_1}$
θ	boundary layer momentum thickness
ν	kinematic viscosity
ρ	density

Subscripts

1	upstream conditions, defined in plane X/C_{ax}=-0.70
2	conditions at the exit of stator, defined in plane X/C_{ax}=1.13
3	conditions at the exit of rotor, defined 0.0104 m downstream of rotor trailing edge
atm	atmospheric conditions
ax	axial direction
H	hub
ℓ	local
MS	mid span
o	total conditions
r	radial direction
R	rotor
s	static conditions
S	stator
T	tip

INTRODUCTION

It is recognized that progress in the research of secondary flows in turbine bladings can be obtained only by simulating as closely as possible the flow conditions existing in the complex environment of real machines. Investigations of the flow field in annular turbine nozzle guide vanes present an important step in this direction. Different investigators [1,4,9,10] emphasized the signi-

ficance of the radial pressure gradient and, mainly in [1], the effects of the radial pressure gradient on the flow field in annular turbine nozzle guide vanes have been studied in great detail by exploring systematically the whole field throughout the cascade passage.

Considering the importance of the downstream conditions for the flow field in annular cascades it is vital that the model test apparatus allows to reproduce the correct radial pressure gradient at the cascade outlet. In a turbine stage the rotor is designed to match the radial pressure gradient set up by the stator and to provide in general a nearly constant radial pressure distribution at the turbine exit. Due to the high expenses in building up a complete turbine stage and the additional complications in carrying out the measurements, most of the tests reported on annular cascades, e.g. [1,3,6,7,10] are conducted with an open outlet, i.e., the flow leaving the guide vane is simply exhausted to a constant pressure chamber (often atmosphere) via an outlet duct. This way is often criticized, e.g. by Vavra in a discussion of a paper by Fiedler [3] and in his book on "Aerothermodynamics and Flow in Turbomachines", pp 167-168. Vavra argued that the constant far downstream pressure can significantly alter the cascade outlet flow conditions and introduce eventually flow separation at the hub end wall. Similar experiences have been made in England as expressed by Spurr in a discussion of a paper by Goldman and MacLallin from NASA [6]. In [8], Denton reports on a novel technique to reproduce the correct radial pressure gradient by using a perforated plate instead of the rotor. Sjolander [4] conducted his measurements turning the flow downstream of the test section back to the axial direction via a row of outlet guide vanes but he reports also that preliminary tests with and without outlet guide vanes apparently did not show any effect on the outlet flow field. Bammert and Kiaukens [5] invesigated both analytically and experimentally the flow in and downstream of an annular cascade with exhaust to a constant pressure chamber and showed that the appearance of a hub endwall boundary layer separation was clearly related to the hub-to-tip ratio and the outlet flow angle, the danger of separation increasing for small hub-to-tip ratios.

The secondary flow investigation carried out at the von Karman Institute [1] on an annular cascade with a hub-to-tip ratio of 0.8 and exhaust to atmospheric pressure via a cylindrical outlet duct followed by a conical diffuser did not show any evidence of boundary layer separation at the hub up to the furthest downstream measurement plane, i.e., at an axial distance of 70% of the axial chord from the trailing edge. This absence of endwall separation is a first indication that the unrealistic far downstream conditions did not influence fundamentally the flow field near the cascade. A further confirmation that the presence of a downstream rotor should not modify profoundly the outlet flow field is given by Van Hove [11]. The author compares the measured flow field presented in [1] with a 3D, inviscid, rotational flow calculation imposing at the downstream boundary the radial equilibrium condition. Figure 1 shows this comparison for the spanwise static pressure distribution at $0.11 \times C_{ax}$ distance from the trailing edge plane (this plane is of immediate interest for this paper but not shown in [11]). The agreement is rather good, but this is not a definite proof that the outlet flow in the experiment was not influenced at all by the far downstream conditions.

In fact, in establishing the correct outlet conditions, the downstream rotor introduces also a change of the meriodional streamline curvature. At low speed, the radial flow angles associated with it are small. However, this is not the case for the radial flow angles within the wake, which can take considerable proportions. Hence it cannot be excluded that the rotor might have a non negligible influence on the radial loss migration.

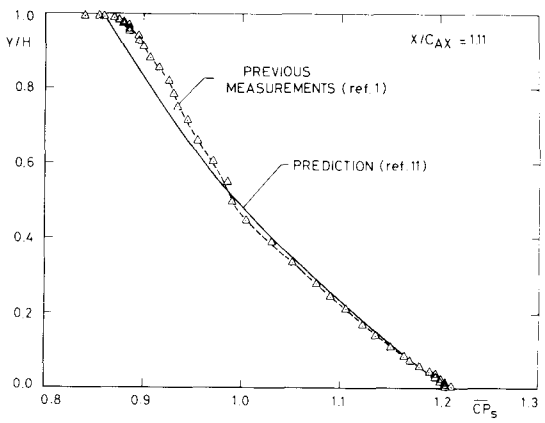

Fig. 1-Comparison of the spanwise CP_s distribution as measured [1] and predicted by a 3D, inviscid, rotational flow calculation (X/C_{AX} = 1.11)

Another possible rotor effect could result from the generation of endwall boundary layer skew upstream of the rotor through the scraping effect of the rotor blades and the rotor disc.

In order to eliminate any doubts and in the absence of any similar experiment, a test program was set up to evaluate the effect of a downstream rotor on the outlet flow field of an annular turbine nozzle guide vane and moreover to separate possible effects of the rotor blades from that of the rotating rotor disc. The flow is explored by means of a double head four hole probe in a measurement plane behind the turbine nozzle guide vane.

EXPERIMENTAL FACILITY

The tests were carried out in the VKI open loop low speed turbine test rig. The rig has been designed to study different test section configurations. Previous studies in the same test rig include the investigation of the 3D field field in an annular turbine nozzle guide vane with a collateral inlet endwall boundary layer [1] and the effects of a skewed inlet endwall boundary layer on the above flow field [10]. The test configuration used for the present investigation is shown in figure 2.

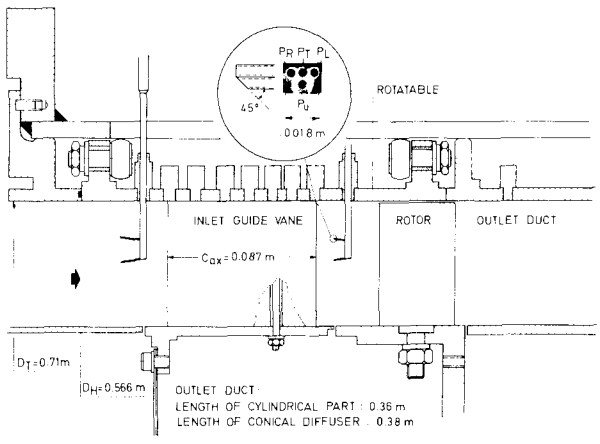

Fig. 2 - Test section

A low aspect ratio stator (H/C=0.6) is followed by a rotating blade row of an aspect ratio H/C=1.2. Both hub and tip endwalls are cylindrical with diameters of 0.566 m and 0.71 m respectively. An effort has been made to simulate correctly the position of the rotor relative to

the stator, often taken in real machines equal to the stator throat. Due to the short distance between stator and rotor, the outlet flow field could be surveyed in one plane only. This plane was chosen to be as close as possible to the first downstream plane of the tests reported in [1]. The axial clearance between stator hub endwall and rotating rotor disc is kept as small as possible. It varies from a minimum of 0.2 mm to a maximum of 0.4 mm. The measurement plane is positioned slightly ahead of this gap. Upstream of the stator a cylindrical inlet duct of 0.57 m length generates an inlet endwall boundary layer of representative thickness. Downstream of the rotor, the flow is exhausted to the atmosphere via a cylindrical duct of 0.36 m length and a conical diffuser of 0.38 m length. The power of the rotor is absorbed by a double-disk water brake dynamometer mounted on the shaft of the turbine rotor at the exit of the conical diffuser.

The test arrangement allows to replace the turbine rotor by a rotating hub endwall having exactly the same geometry as the rotor disk. This "unbladed rotor" is driven by a small DC motor replacing the water brake dynamometer.

Details of the experimental procedure are given in[1].

BLADE AND CASCADE GEOMETRY

The blade and cascade geometry at mid blade height for the configuration with downstream rotor is shown in figure 3. The turbine stator has a constant profile over the blade height and is untwisted. The blade coordinates

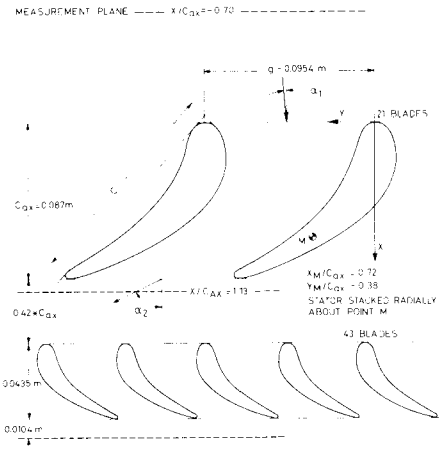

Fig. 3 - Cascade geometry at mid blade height

are given in [1]. Since the main purpose of the rotor is to set up the correct radial pressure gradient, it was decided that an untwisted rotor blade of constant blade section along the height would be adequate. The rotor blade profile is the same as for the stator. The only difference with respect to the stator blade is a reduced chord length : C_R/C_S=0.50. Evidently the rotor does not work at optimum incidence along the whole blade height. However, the inlet angle variation from hub to tip remains within acceptable limits at tne nominal working point (see test conditions). The most important geometrical characteristics of the fixed and the rotating blade row are summarized below. The rotor disk of 0.075 m total axial width extends from 0.0245 m upstream of the rotor leading edge to 0.007 m downstream of the rotor trailing edge.

NOTE : angles are given with respect to axial direction. Relative to each blade row, the angles are given positive when pointing from blade pressure side to suction side. The stator blade is stacked radially about point M (Fig.3).

A tripping wire of 0.2 mm diameter was placed on the blade suction side at X/C=0.35 (chordwise position) [1].

	STATOR	ROTOR
-tip diameter, D_T	0.710 m	0.710 m
-hub diameter, D_H	0.566 m	0.566 m
-chord length, C	0.12 m	0.06 m
-axial chord length, C_{ax}	0.087 m	0.0435 m
-aspect ratio, H/C	0.6	1.2
-number of blades, N	21	43
-pitch to chord ratio at hub,mean and tip	0.706;0.795; 0.885	0.689;0.777; 0.866
-inlet blade angle, α_1	-7	-7
-arc cos(O/g) at hub, mean and tip (measured values)	69.0°;67.3°; 66.2°	69.1°;68.0°; 67.0
-tip clearance	-	0.0012 m
-axial distance between stator & rotor blades	-	0.0365 m

TEST PROGRAM AND OVERALL TEST CONDITIONS

Test program

The test program consisted of three series of measurements :
(a) tests with downstream rotor,
(b) tests with rotating unbladed rotor disks,
(c) tests with stationary unbladed rotor disk.
Test series (c) is not just a repeat of the previous experiments in [1]. It differs from [1] by the clearance separating the rotor disk from the hub endwall. In order to isolate properly the rotational effect of the rotor disk, it seemed necessary to avoid any secondary effects due to difference in the geometry of the endwall. Also, the position of the downstream measured plane differs slightly from that in [1] due to the use of a different probe.

The measurements for all three cases included the survey of the flow in a plane far upstream of the stator leading edge (X/C_{ax}=-0.70) and in a plane slightly downstream of the trailing edge of the stator (X/C_{ax}=1.13). The distances are given with respect to the stator leading edge plane. At X/C_{ax}=-0.70, where the flow is circumferentially uniform, 6 radial traverses were made. The measurements at X/C_{ax}=1.13 include 18 radial traverses covering a stator pitch. The flow periodicity at the exit of the stator was checked in [1]. For case (a), the flow was also surveyed downstream of the rotor by 9 radial traverses distributed equally over a circumferential distance equal to a stator pitch. Test results reported in [9] and [12] show in fact a circumferential variation of the rotor outlet flow with respect to the position of the stator blades. Each of the above traverses from tip to hub endwall contains 35 measuring points. The data were recorded on magnetic tape and processed on a PDP 11/34 computer.

The test conditions are summarized in the following table.

Upstream of the stator : X/C_{ax} = -0.70 mid span

	Tests (a)	Tests (b),(c)
-total temperature, T_{t1}	288 K	288 K
-total pressure, P_{t1}	P_{atm}+141.5 mm H$_2$O	P_{atm}+70 mm H$_2$O
-flow angle in blade-to-blade plane, α_1	0.3°	0.7°
-radial flow angle, γ_1	0°	0
-velocity, V_1	14.5 m/s	12.5 m/s
-Reynolds number, Re_1	$1.14 \cdot 10^5$	$0.98 \cdot 10^5$
-turbulence, Tu	0.8%	0.8

Downstream of the stator : X/C_{ax} = 1.13

	Tests (a)	Tests (b),(c)
-static pressure, $P_{s2,HUB}$	P_{atm}+45 mm H_2O	P_{atm}-7 mm H_2O
-Reynolds number, Re_2 (at mid span)	2.85×10^5	2.45×10^5
-inlet flow angle relative to the rotor blade at Y/H=0.2;0.5;0.8	-10.2°;+2.5°; +16.8°	

Downstream of the rotor (0.0104 m from rotor trailing edge) :

	Tests (a)
-absolute flow angle, α_3 (at mid span)	9°
-static pressure, P_{s3} (at mid span)	P_{atm}+7.8 mm H_2O

NOTE : the static pressure field is radially uniform.

The rotational speed of the rotor (tests (a)) is N=1000 RPM.

The rotational speed of the rotating unbladed rotor disk (tests (b)) is taken N=875 RPM in order to have the same ratio of the peripheral velocity of the rotating hub over the axial component of the velocity, U_H/V_{ax}, as for tests (a).

Upstream conditions

The radial distribution of the mass averaged total pressure coefficient $\overline{CP}_0$ at the far upstream plane X/C_{ax} =-0.70 is presented in figure 4. The inlet endwall boundary layer characteristics are presented in the following table.

Tip endwall :	Tests (a)	Tests (b),(c)	Ref. [1]
δ/H	0.16	0.16	0.15
δ^*/H	0.021	0.022	0.025
θ/H	0.016	0.017	0.019
$H_{1,}$	1.33	1.29	1.33

Hub endwall :	Tests (a)	Tests (b),(c)	Ref. [1]
δ/H	0.13	0.12	0.11
δ^*/H	0.019	0.017	0.017
θ/H	0.013	0.010	0.010
$H_{1,}$	1.41	1.67	1.67

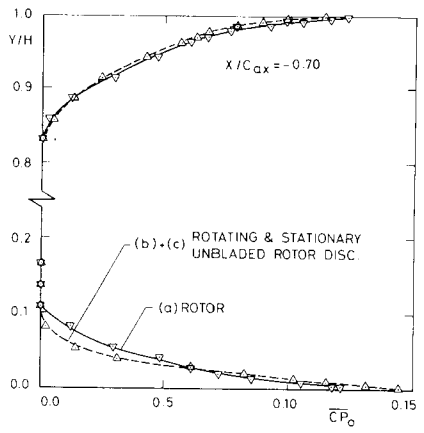

Fig.4 - Spanwise distribution of the total pressure loss coefficient $\overline{CP}_0$ (X/C_{ax} = -0.70)

The overall loss $\overline{\overline{CP}}_0$ at X/C_{ax}=-0.70 is measured equal to 0.8% for tests (a) and 0.7% for tests (b) and (c). The tip endwall boundary layer is fully turbulent for both tests. The hub endwall boundary layer is in a transitional state during tests (b) and (c) but nearly fully turbulent for tests (a). This is partially explainable by the higher value of the upstream velocity during tests (a), moving the beginning of the hub endwall boundary layer transition upstream.

The differences of the hub endwall boundary layer characteristics appeared to be non negligible for a correct comparison between test series (a) and (b)+(c),since they imply a different normal vorticity distribution at the inlet, which might be sufficient to affect the downstream angle distribution. Calculations with a 3D, inviscid,rotational calculation method [11] showed that the difference would result for series (a) in a linear increase of the overturning from 0° at Y/H=0.14 to 0.6° at Y/H=0.007 (first calculation point).

Experimental accuracy

The measuring accuracies associated with the four hole probes are as follows :

- radial position of probe ± 0.1 mm
- axial and tangential position of probe ± 0.5 mm
- total pressure coefficient, CP_0 ± 0.01
- static pressure coefficient, CP_s ± 0.02
- flow angle in blade-to-blade plane, α ± 0.8°
- radial flow angle in streamwise direction ± 1°

Note that the measuring accuracy for the radial flow angle deteriorates for distances from the wall smaller than 2 mm.

It should be mentioned that in addition to the direct measurement errors, integrated values may be in error due to a lack of data points in regions with high gradients. A typical example is the pitch-averaged wake losses outside the secondary flow regions. With 18 radial traverses in the downstream plane there are only 3 to 4 points in the wake region. The number is insufficient to evaluate correctly the wake losses and the integrated values have to be taken with some precaution.

EXPERIMENTAL RESULTS

The experimental results are presented in a way to facilitate the comparison not only between the three present tests but also with the results of the tests reported in [1]. Both spanwise pitch-averaged distributions and contour plots are shown. The total and static pressures are presented in the form of pressure coefficients CP_0 and CP_s. As in [1], the radial flow angle γ is calculated from the ratio of radial and axial velocity components : γ = arctg V_r/V_{ax}.

We also note that, due to the high values of the downstream flow angle in the blade-to-blade plane α_2, the absolute value of the radial angle is considerably bigger than the flow inclination measured in the streamwise direction. An error of one degree in the radial angle in the streamwise direction amounts to about 2°→3° error after after projection in the meridional plane.

Spanwise pitch-averaged distributions of flow angle, total and static pressure

Comparison of the previous results [1] with tests (c) (stationary rotor disk)

Figures 5a,b,c present a comparison of the spanwise pitch-averaged distributions of flow angle, total and static pressure of tests (c) (downstream stationary rotor disk) with the results reported in [1]. Figure 5a presents as additional information the flow angle distribution at X/C_{ax}=1.68 of the tests reported in [1]. We remind that the small circumferential gap at X/C_{ax}=1.145 at the

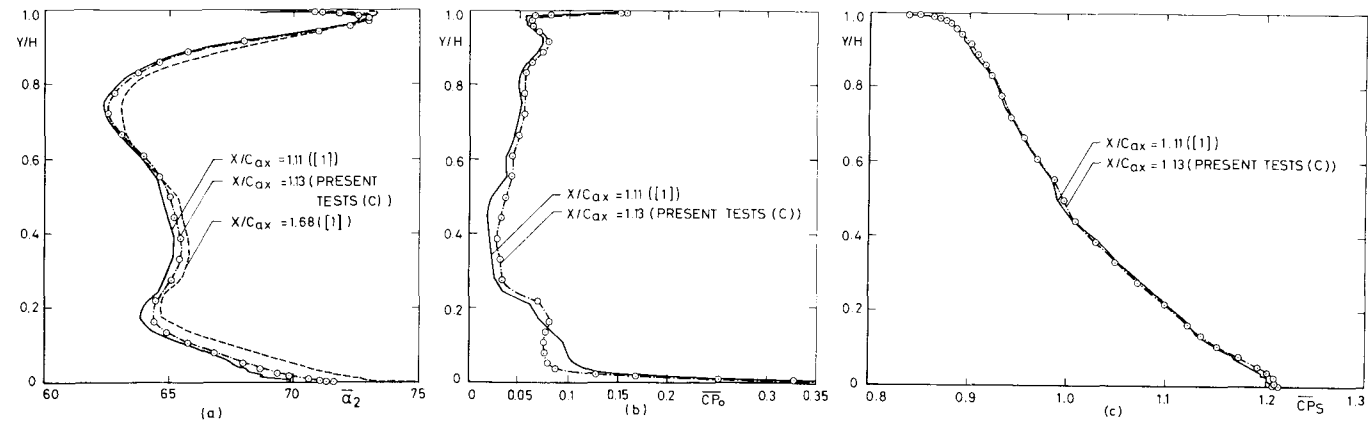

Fig. 5 - Comparison of the spanwise distributions of flow angle, total pressure and static pressure as measured during the present tests (c) and reported in [1]

hub endwall and the slight difference in the location of the measurement planes are the only changes between the two test series.

The spanwise distributions of the flow angle $\overline{\alpha_2}$ are in very good agreement (Fig. 5a) and the static pressure distributions are practically identical (Fig. 5c). Thus we can conclude that the gap does not influence either of them. The loss distributions show rather good agreement for the upper half of the span where the differences are within the measurement accuracy. The difference around midspan, but in a general way all differences in wake losses outside the secondary flow regions, are most probably to be attributed to a lack of data points in the high total pressure gradient region, as already explained in the section on measurement accuracy. The differences in the spanwise loss distribution near the hub are more difficult to explain. It seems that they present rather a redistribution of the losses than a change of their total amount.

Effects of rotor blades and unbladed rotor disk

The spanwise distribution of the flow angle α and the total and static pressure coefficients CP_0 and PC_S for the test series (a), (b) and (c) are presented in figures 6a-c.

Within the measurement accuracy the static pressure (Fig. 6c) is the same for all three configurations except at the hub within a distance of 5% to 10% of the span. Both tests with rotor and with the unbladed rotor disk show in this region a definite rise of the static pressure, i.e., a decrease of the CP_S, with respect to the stationary rotor disk. On the other hand, Fig. 5c did show that by comparison with the tests in [1] the gap between the stator endwall and rotor disk alone did in a way affect the static pressure distribution. Figure 6c suggests therefore that the observed pressure difference is due to the rotation of the rotor disk rather than due to the blade. This seems to be confirmed by the fact that the rotor blades do not cause any changes at the tip endwall which could be attributed to them.

Next, let us turn to the spanwise loss distribution (Fig. 6a). Again it should be kept in mind that the measurements of the losses outside of the secondary loss regions suffer from the limited number of points in the wake. This is clearly demonstrated by the fact that all CP_0-values between Y/H=0.25 and 0.80 lie within a bandwidth of ±0.6% (absolute losses) without showing any definite trends. On the contrary, the loss distributions at the tip endwall differ very little from each other, indicating that the presence of the rotor blades does not significantly influence the spanwise secondary loss distribution. Of course, it is not likely that the rotating unbladed rotor disk could introduce any modifications at all in this region. The good agreement between the tests with stationary and rotating rotor disk can therefore be taken as a sign for the good repeatability of the tests. The situation at the hub endwall secondary loss core is somewhat different. Between Y/H=0.25 and 0.12 there is an excellent agreement between all three curves, however, at about Y/H=0.08 both the rotor and the rotating unbladed rotor disk curves are characterized by a drop in CP_0 of 1.2 to 2 points, the higher value being recorded for

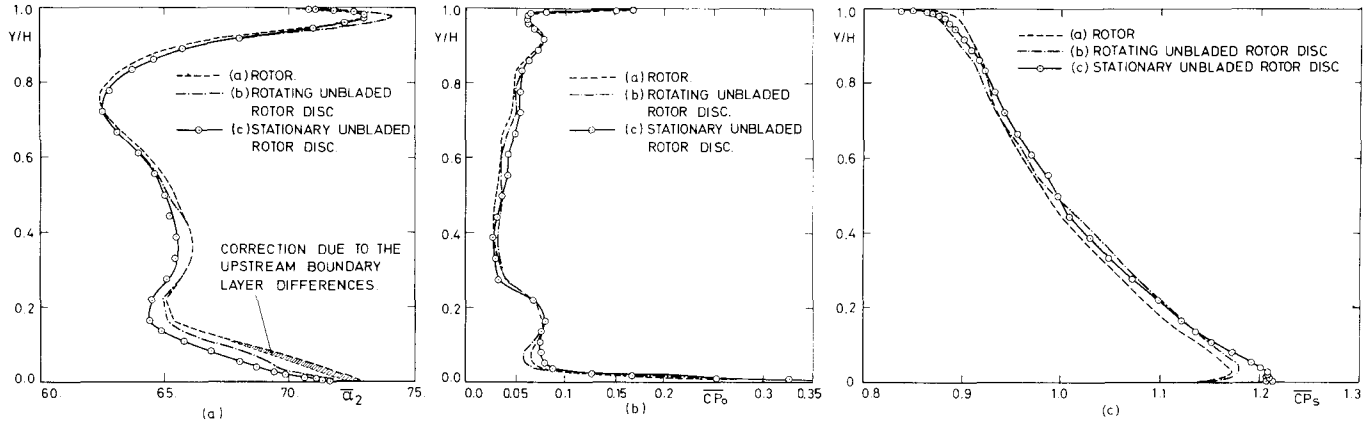

Fig. 6 - Effects of the rotor blades and the unbladed rotor disk on the spanwise distribution of flow angle, total pressure and static pressure

the rotating unbladed rotor disk. Similar as in the case of the static pressure, it appears that the rotational effect of the rotor disk is more important than the effect of the rotor blades, but again the effect is rather limited.

As far as the flow angle, α, is concerned, we notice first of all the very small differences of all curves in the upper half span, except for a very local deviation of about 1.2° of the curve for the rotating rotor disk at $Y/H \cong 0.98$. This can only be explained by a measuring error since it is excluded that this is a real flow effect. The rotor blades impose not even the slightest outlet angle variation. For the lower half span the analysis is more problematic. Both the curves for the rotor and the rotating unbladed rotor disk start to show higher α-values for $Y/H<0.5$. Down to $Y/H=0.2$ there is an almost constant difference of 0.7° which is in fact within the measuring accuracy although one might expect that the accuracy of pitch-integrated values should be higher than that of a local angle measurement. For $Y/H<0.2$ the curves for the rotor and the rotating unbladed rotor disk start to diverge, with slightly higher α-values for the rotor ($\sim$1° to 1.5°) while the curve for the rotor disk takes an intermediate position with an almost constant difference of $\Delta\alpha=+1°$ with respect to the stationary rotor disk curve. The rotor curve has still to be corrected due to the effect caused by a different inlet boundary layer. As indicated before this has been done using a 3D, rotational, inviscid flow calculation method. This correction (see Fig. 6a) takes a maximum value of 0.6° at the wall and decreases almost linearly to zero at $Y/H=0.14$. In conclusion, for $Y/H<0.2$ the α-angle for the rotating disk is by $\sim$1° higher than for the stationary disk and the curve for the rotor $\sim$1° higher than that of the rotating disk. Measuring errors can explain partially the differences but hardly all.

Contour plots of total pressure, static pressure and radial flow angle

Since the spanwise distributions have shown that all the effects of the rotating unbladed rotor disk are included in the effects of the rotor, we restrict the comparison of the flow contours only to tests (a) and (c). The contour plots of total pressure, static pressure and radial flow angle for the above two tests are presented in Fig. 7. The amount of new information given by comparing the two tests (Fig. 7) is rather limited; the same basic flow patterns are mainly observed.

As far as the static pressure is concerned, we notice that the biggest differences occur within the wake region and to the right of it (i.e., pressure side of the wake). A check of the pitchwise static pressure distributions at various radii indicated that the most important differences appeared as a rather local pressure increase in the wake of the order of 5-10% of the CP_s-values. Except in the hub region, these differences are too small to significantly affect the pitch-averaged values. A comparison of the pitchwise distribution of the static pressure with downstream rotor to that obtained with the unbladed rotating rotor disk did not show any particular pressure differences across the wake but rather differences of the order of the measuring accuracy (±0.02 of CP_s-value) distributed smoothly along the entire pitch which explains the differences between the two test series in the spanwise static pressure distribution in Fig. 6c. This seems to indicate the possibility that a local change of the static pressure distribution at the hub caused by the rotating rotor disk alone could eventually be transmitted all through the wake to the tip, without being in the pitch-averaged spanwise distribution of the static pressure.

Keeping in mind a measuring accuracy of ±2° for the radial flow angle after projection into the meridional plane (±0.8° in streamwise direction), it appears that the only noteworthy change introduced by the downstream rotor is a local reduction of the inward flow at the region of maximum losses near the hub. This could be explained by the centrifugal effect of the rotor disk, which can be expected strongest within a high loss region.

As far as the total pressure loss contours are concerned, the most noticeable difference between the two test series is a broadening of the wake from the hub to about 60% of the blade height with downstream rotor.

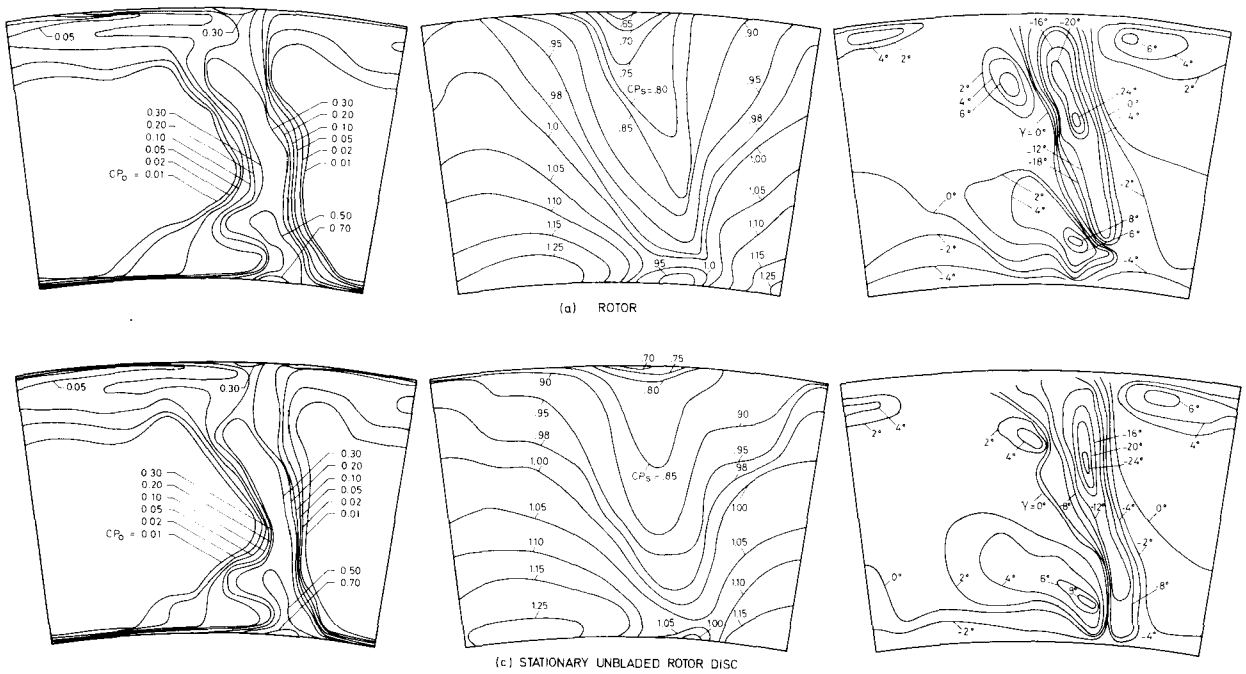

Fig.7-Contour plots of losses,static pressure and radial flow angle distribution at $X/C_{ax}=1.13$ (Tests (a) and (c))

Whether this can be related to the static pressure rise in the wake region is not certain.

Overall losses and mass flow coefficient

The overall losses $\overline{\overline{CP}}_0$ measured at the plane X/C_{ax}= 1.13 are 5.2%, 5.5% and 5.6% for tests (a),(b) and (c) respectively. These values include an inlet endwall boundary layer loss of 0.8%, 0.7% and 0.7%. The overall losses reported in [1] are 5.4% at X/C_{ax}=1.11 and 7.2% at X/C_{ax}=1.68. The small differences of the above mentioned values at X/C_{ax}=1.13 could be due to the experimental error. The higher Reynolds number during tests (a) could also have a slignt contribution on the lower value of losses with downstream rotor.

The mass flow coefficient, η, defined as the ratio of the mass flow downstream of the stator over the upstream mass flow is 1.05, 1.06 and 1.05 for tests (a),(b) and (c). These values are very sensitive to systematic errors in measuring the upstream static pressure and the outlet flow angle. A ±3% error of the mass flow coefficient could be caused by errors of the outlet flow angle measurement equal to the measuring accuracy; an error of the same order of magnitude can be expected from errors involved in the measurement of the upstream static pressure. Reported values from measurements in plane cascades situate the discrepancies at the inlet-outlet mass flow rates on the same level (5% by Langston in [13] and 8.6% by Moore and Ransmayr in [14]).

CONCLUSIONS

1. The presence of a downstream rotor introduced local changes to the outlet flow field of an annular cascade with a hub-to-tip ratio of D_H/D_T=0.8 and about 65° outlet flow angle, but no fundamental modifications were observed.
2. These changes appear to be due to the effect of rotating rotor disk than due to the rotor blades.
3. Except for a moderate static pressure rise of 5-10% throughout the entire wake region, all changes are limited to the lower half span. Within the extension of the secondary flow region, local moderate changes may occur for all flow values.
4. The pitch-averaged spanwise distributions show only minor changes close to the hub; about 5% for the static pressure, 1° to 2° for the overturning and a local drop of ∿1% for the losses. The overall losses are not affected.
5. It is possible to carry out high hub-to-tip ratio annular nozzle tests without a downstream rotor if the outlet diffusing duct is long as in the present case. The above conclusions might not be necessarily applied to nozzles with considerably higher outlet flow angles.

ACKNOWLEDGEMENTS

The authors wish to thank Dr T. Arts for his help running the computational code. Mr P. de Pret and Mr B. Thiery participated at the experimental work.

REFERENCES

1. Sieverding,C.H;Van Hove,W.;Boletis,E.: Experimental study of the 3D flow field in an annular turbine nozzle guide vane. ASME P 83GT120; also VKI Preprint 1982-38.
2. Vavra,M.H.: Aero-thermodynamics and flow in turbomachines. New York, R. Krieger Publ. Co., 1974.
3. Fiedler,K.: To the more dimensional calculation of axial turbomachines. in "Proceedings of the Seminar on Advances Problems in Turbomachinery", VKI LS 1, Part 1, March 1965.
4. Sjolander,S.A.: The endwall boundary layer in an annular cascade of turbine nozzle guide vanes. Carleton University, TR ME/A 75-4, December 1975.
5. Bammert,K. & Kläukens,H.:Nabentotwasser hinter Leiträdern von axialen Strömungsmaschinen. Ingenieur-Archiv, Band XVII, 1949, pp 367-390.
6. Goldman,L.J. & McLallin,K.L.: Effect of endwall cooling on secondary flow in turbine stator vanes. in "Secondary Flows in Turbomachines", AGARD CP 214, 1977.
7. Haas,J.: Analytical and experimental investigation of stator endwall contouring in a small axial flow turbine. I-Stator performance. NASA TP 2023, 1982.
8. Denton,J.D.: A review of current research activity on the aerodynamics of axial flow turbines. in "Aerothermodynamics of Low Pressure Steam Turbines and Condensors", VKI LS 1983-06, May 1983.
9. Hunter,I.H.: Endwall boundary layer flows and losses in an axial turbine stage. ASME Transact., Series A : J.Engrg for Power, Vol. 104, No 1, Jan. 1982, pp 184-193.
10. Boletis,E.;Sieverding,C.H.;Van Hove,W.: Effects of a skewed inlet endwall boundary layer on the 3D flow field in an annular turbine cascade. in "Viscous Effects in Turbomachines". AGARD CP 351, Paper 16, 1983; also VKI Preprint 1983-12.
11. Van Hove, W.: Calculation of 3D, inviscid, rotational flow in axial turbine blade rows. ASME P 83GT119; also VKI Preprint 1983-10.
12. Whitney,N.J.;Buckner,J.;Monroe,D.E.: Effect of nozzle secondary flows on turbine performance as indicated by exit surveys of a rotor. NACA RM E54B03, April 1954.
13. Langston,L.S.;Nice,M.L.;Hooper,R.M.: 3D flow within a turbine cascade passage. ASME Transact., Series A : J.Engrg for Power, Vol. 99, No 1, Jan.1977, pp21-28.
14. Moore,J. & Ransmayr,A.: Flow in a turbine cascade. Part I - Losses and leading edge effects. ASME P 83GT68.